

The High-Pressure Modification of CePtSn – Synthesis, Structure, and Magnetic Properties

Jan F. Riecken^a, Gunter Heymann^b, Theresa Soltner^b, Rolf-Dieter Hoffmann^a,
Hubert Huppertz^b, Dirk Johrendt^b, and Rainer Pöttgen^a

^a Institut für Anorganische und Analytische Chemie, Westfälische Wilhelms-Universität Münster,
Corrensstraße 36, D-48149 Münster (Germany)

^b Department Chemie und Biochemie, Ludwig-Maximilians-Universität München,
Butenandtstraße 5–13 (Haus D), D-81377 München (Germany)

Reprint requests to R. Pöttgen. E-mail: pottgen@uni-muenster.de

Z. Naturforsch. **60b**, 821 – 830 (2005); received June 15, 2005

The high-pressure (HP) modification of CePtSn was prepared under multianvil high-pressure (9.2 GPa) high-temperature (1325 K) conditions from the normal-pressure (NP) modification. Both modifications were investigated by powder and single crystal X-ray data: TiNiSi type, *Pnma*, $a = 746.89(9)$, $b = 462.88(4)$, $c = 801.93(7)$ pm, $wR2 = 0.0487$, 452 F^2 values, 20 variable parameters for NP-CePtSn, and ZrNiAl type, *P62m*, $a = 756.919(5)$, $c = 415.166(4)$ pm, $wR2 = 0.0546$, 252 F^2 values, 14 variable parameters for HP-CePtSn. Both modifications are built up from platinum-centered trigonal prisms. Together, the platinum and tin atoms form different three-dimensional [PtSn] networks in which the cerium atoms fill channels. The crystal chemistry and chemical bonding of NP- and HP-CePtSn is discussed. Susceptibility measurements of HP-CePtSn indicate Curie-Weiss behavior above 40 K with an experimental magnetic moment of 2.55(1) μ_B /Ce atom, indicating trivalent cerium. No magnetic ordering could be detected down to 2 K.

Key words: High-Pressure, Intermetallics, Magnetism, Crystal Structure

Introduction

The equiatomic cerium intermetallics CeTX ($T =$ transition metal; $X =$ element of the 3rd, 4th, or 5th main group) have attracted considerable interest of solid state chemists and physicists in the last 15 years, due to the large variations in the magnetic and electrical properties, such as mixed cerium valency, Kondo behavior, ferro- or antiferromagnetic ordering, metamagnetism, or heavy Fermion behavior. An overview of the many compounds is given in [1–4].

A peculiar compound in the series of these CeTX intermetallics is the stannide CePtSn which was synthesized for the first time by Sakurai *et al.* [5]. The orthorhombic TiNiSi type structure was evident from the X-ray powder data. In a subsequent single crystal study Higashi *et al.* [6] assigned a non-centrosymmetric variant of the TiNiSi type in space group *Pna2*₁. Subsequent X-ray and neutron diffraction studies [7–9] again confirmed the centrosymmetric TiNiSi type structure.

CePtSn has intensively been studied with respect to the outstanding magnetic and electrical properties [10–49]. This stannide is a metallic Kondo lattice ma-

terial which orders antiferromagnetically around 8 K and shows an additional magnetic phase transition at 5.5 K. Neutron powder and single crystal data showed incommensurate magnetic ordering of the cerium magnetic moments [7, 9, 15, 29]. The magnetic structure seems to depend on the nature of the sample [9]. Inelastic neutron scattering showed well defined crystal field excitations at 24.0 and 34.9 meV [24]. In the magnetically ordered state, a transferred hyperfine field of 12 T at the tin nuclei can be detected at 1.5 K in the ¹¹⁹Sn Mössbauer spectra [25].

All these investigations were carried out under ambient pressure conditions. We have studied CePtSn under high-pressure/high-temperature conditions. NP-CePtSn with TiNiSi type structure transforms to HP-CePtSn with ZrNiAl type structure at 9.2 GPa and 1325 K. The characterization of the structure and the magnetic properties of the high-pressure modification are reported herein.

Experimental Section

Synthesis

Starting materials for the preparation of NP-CePtSn were cerium ingots (Johnson Matthey, > 99.9%), platinum pow-

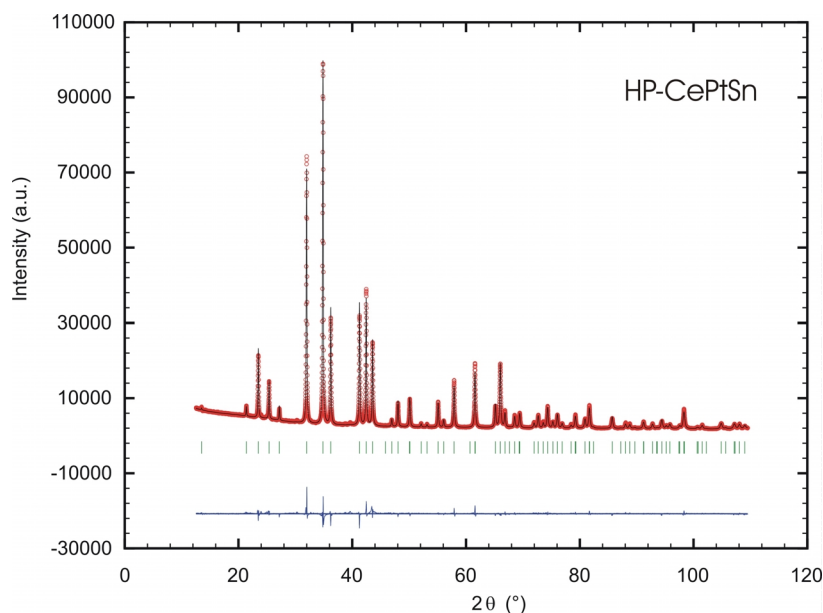


Fig. 1. Rietveld refinement plot for HP-CePtSn in which the observed intensities are indicated with open circles and the calculated pattern with a line on top of the circles. The vertical lines indicate the Bragg positions. The difference $I(\text{obs})-I(\text{calc})$ is drawn below the Bragg indicators.

der (Degussa-Hüls, 200 mesh, > 99.9%), and tin granules (Heraeus, > 99.999%). The larger cerium ingots were first cut into smaller pieces under paraffin oil and subsequently washed with *n*-hexane. The paraffin oil and *n*-hexane were dried over sodium wire. The small cerium pieces were then arc-melted [50] to small buttons (*ca.* 500 mg) under an argon atmosphere of *ca.* 800 mbar and kept under argon in Schlenk tubes prior to the reactions. The argon was purified over silica gel, molecular sieves, and titanium sponge (900 K). The pre-melting procedure for cerium strongly reduces shattering during the exothermic reaction with platinum and tin.

A cerium button was then mixed with a cold-pressed pellet of platinum and pieces of the tin granules in the ideal 1:1:1 atomic ratio and arc-melted under an argon pressure of about 800 mbar. The product button was remelted three times in order to ensure homogeneity. The total weight-loss after the melting procedures was smaller than 0.5 weight-%. The purity of the NP-CePtSn sample was studied *via* powder X-ray diffraction (see below). NP-CePtSn melts congruently.

The high-pressure/high-temperature treatment took place *via* a multianvil assembly. Details concerning the construction of the assembly can be found in references [51–54]. A boron nitride crucible of an 18/11-assembly was loaded with carefully milled NP-CePtSn, compressed within 4 h to 9.2 GPa and heated to 1000 °C for the following 20 min. After holding this temperature for 3 min the sample was cooled down to 500 °C within a minute. Subsequent annealing under pressure at 500 °C for 50 min enhanced the crystallinity of the sample and was followed by quenching to room temperature. After decompression, the sample was carefully sep-

arated from the surrounding assembly parts and obtained as a single phase product.

NP-CePtSn and HP-CePtSn are stable in moist air over weeks. The polycrystalline samples are silvery with metallic luster. Powdered samples of both modifications are dark gray.

X-ray powder data of NP-CePtSn

NP-CePtSn was characterized through a Guinier powder pattern using Cu- $K\alpha_1$ radiation and α -quartz ($a = 491.30$, $c = 540.46$ pm) as an internal standard. The Guinier camera was equipped with an image plate system (Fujifilm BAS-1800). The indexing of the pattern was facilitated by an intensity calculation [55] using the atomic parameters of the refined structure. The orthorhombic lattice parameters (Table 1) were obtained by least-squares fits of the Guinier data. The powder data compare well with the previous literature data [6, 8, 9].

Rietveld refinement of HP-CePtSn

The polycrystalline sample prepared under high-pressure high-temperature conditions was investigated on a powder diffractometer (Stoe Stadi P, Cu- $K\alpha_1$ radiation) in order to perform a full profile Rietveld refinement. The data are presented in Fig. 1. The measurement was performed in transmission geometry with a flat sample using Cu- $K\alpha_1$ radiation ($\lambda = 154.0598$ pm, Ge monochromator). All experimental details are listed in Table 1.

The Rietveld calculations were performed with the FULLPROF [56] software. The background was set manually and the profiles were modelled using the pseudo-Voigt function.

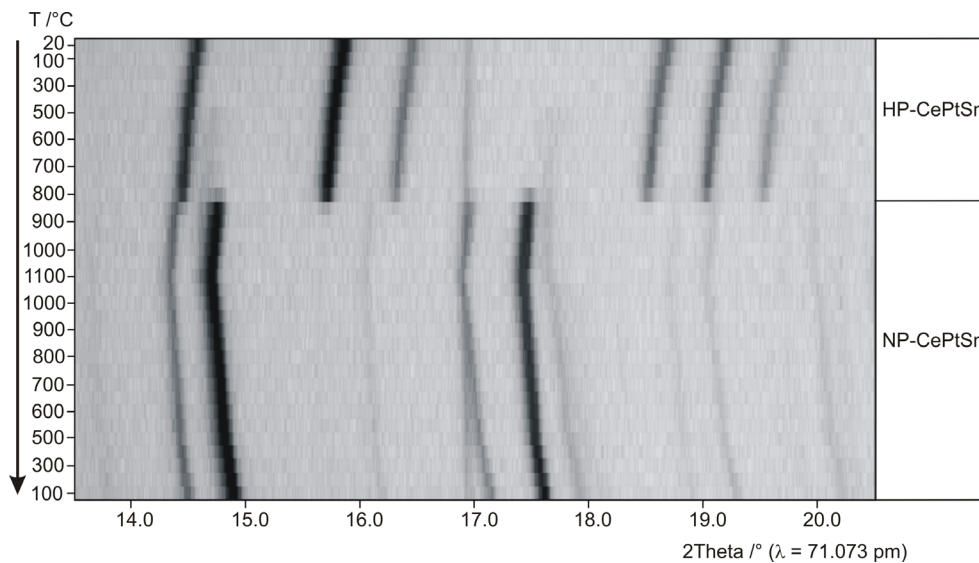


Fig. 2. Temperature-dependent X-ray powder patterns of HP-CePtSn. The continuous line at $2\theta \approx 17^\circ$ results from the oven setup.

Table 1. X-ray powder data (Cu- $K\alpha_1$, $\lambda = 1.54051 \text{ \AA}$) and structure refinement for HP-CePtSn ($P\bar{6}2m$, $Z = 3$).

Empirical formula	CePtSn
Formula weight [g/mol]	453.91
Lattice parameters (diffractometer data)	$a = 756.919(5) \text{ pm}$ $c = 415.166(4) \text{ pm}$ $V = 0.2060 \text{ nm}^3$
Calculated density [g/cm ³]	10.98
Absorption correction [μR]	0.70
$F(000)$	558
Range in 2θ	10–110
Scan mode, step width	$\omega/2\theta$, 0.01
No. data points	10000
Total no. Bragg reflections	72
No. structure parameters	8
No. total parameters	14
R_F , R_{wp}	0.037, 0.044
$R_{\text{Bragg}(I)}$	0.053
Bérar-Lelann Factor	5.66

An arbitrary absorption value of $\mu R = 0.7$ has been used. The experimental data of the refinement are summarized in Table 1. The standard deviations of the refined parameters have been multiplied with the Bérar-Lelann factor [57]. The resulting positional parameters are listed in Table 3. The standard deviations of the x parameters for the rare earth metal and the tin position are similar to the single crystal data. The powder data fully confirm the HP structure and show that the sample is very pure on the level of X-ray powder diffraction.

In-situ powder diffraction

To investigate the high-temperature behavior of the intermetallic high-pressure phase CePtSn, temperature depen-

dent *in-situ* X-ray diffractometry was performed on a STOE Stadi P powder diffractometer (Mo- $K\alpha$; $\lambda = 71.073 \text{ pm}$) with a computer-controlled STOE furnace. An electrically heated graphite tube held the sample capillary vertical with respect to the scattering plane. Bores in the graphite tube permitted unobstructed pathways for the primary beam as well as for the scattered radiation. The temperature, measured by a thermocouple in the graphite tube, was kept constant within $0.2 \text{ }^\circ\text{C}$. The heating rate between different temperatures was set to $50 \text{ }^\circ\text{C}/\text{min}$ and the data acquisition started directly after reaching the next temperature step.

Successive heating of HP-CePtSn showed that the high-pressure modification is stable up to $500 \text{ }^\circ\text{C}$ in an argon atmosphere (Fig. 2). The complete transformation into the normal pressure modification takes place at about $850 \text{ }^\circ\text{C}$. No further transformations could be detected, when heating up the sample to $1100 \text{ }^\circ\text{C}$ followed by lowering the temperature to ambient conditions. The consistent low intensity reflection near 17° is an artifact of the oven setup. The same experiment with a capillary under air led to the analogous transformation of the metastable high-pressure phase into the normal-pressure modification, followed by oxidation reactions leading to CeO_2 , SnO_2 , and platinum metal at about $850 \text{ }^\circ\text{C}$.

Single crystal structure refinements

Small irregularly-shaped single crystals of NP- and HP-CePtSn were isolated from the arc-melted sample and the material prepared under high-pressure high-temperature conditions. The crystals were glued onto thin glass fibres with bees wax and first examined on a Buerger precession camera (equipped with an imaging plate system Fujifilm BAS-

Table 2. Crystal data and structure refinement for NP- and HP-CePtSn.

Empirical formula	CePtSn	
	normal-pressure	high-pressure
Molar mass	453.90 g/mol	453.90 g/mol
Space group; <i>Z</i>	<i>Pnma</i> ; 4	<i>P6̄2m</i> ; 3
Structure type	TiNiSi	ZrNiAl
Pearson symbol	oP12	hP9
Unit cell dimensions (powder data)	<i>a</i> = 746.89(9) pm <i>b</i> = 462.88(4) pm <i>c</i> = 801.93(7) pm <i>V</i> = 0.2772 nm ³	<i>a</i> = 756.919(5) pm <i>b</i> = <i>a</i> <i>c</i> = 415.166(4) pm <i>V</i> = 0.2060 nm ³
Calculated density	10.87 g/cm ³	10.98 g/cm ³
Crystal size	10 × 10 × 20 μm ³	20 × 20 × 35 μm ³
Detector distance	–	60 mm
Exposure time	–	5 min
ω Range; increment	–	0–180°; 1.0
Integr. param. A, B, EMS	–	14.0; 4.0; 0.030
Transm. ratio (max/min)	1.61	1.91
Absorption coefficient	75.0 mm ⁻¹	75.7 mm ⁻¹
<i>F</i> (000)	744	558
θ Range	3 to 30°	3 to 30°
Range in <i>hkl</i>	±10; ±6; ±11	±10; ±10; ±5
Total no. reflections	3014	1745
Independent reflections	452	252
<i>R</i> _{int}	0.0644	0.1111
Reflections with <i>I</i> > 2σ(<i>I</i>)	415	228
<i>R</i> _{sigma}	0.0340	0.0756
Data / parameters	452 / 20	252 / 14
Goodness-of-fit on <i>F</i> ²	1.065	0.956
Final <i>R</i> indices	<i>R</i> 1 = 0.0215	<i>R</i> 1 = 0.0363
[<i>I</i> > 2σ(<i>I</i>)]	<i>wR</i> 2 = 0.0474	<i>wR</i> 2 = 0.0536
<i>R</i> Indices (all data)	<i>R</i> 1 = 0.0249	<i>R</i> 1 = 0.0423
	<i>wR</i> 2 = 0.0487	<i>wR</i> 2 = 0.0546
Extinction coefficient	0.0023(3)	0.0031(4)
Flack parameter	–	0.00(3)
Largest diff. peak and hole	1.91 / –2.05 e/Å ³	2.83 / –3.00 e/Å ³

1800) in order to establish suitability for intensity data collection. Intensity data of the HP-CePtSn crystal were col-

lected at room temperature on a Stoe IPDS-II diffractometer with graphite monochromatized Mo-*K*_α radiation. A numerical absorption correction was applied to the data. The NP-CePtSn crystal was measured by use of a four-circle diffractometer (CAD4) with graphite monochromatized Mo-*K*_α (71.073 pm) radiation and a scintillation counter with pulse height discrimination. The scans were taken in the $\omega/2\theta$ mode and an empirical absorption correction was applied on the basis of psi-scan data, followed by a spherical absorption correction. All relevant crystallographic details for the data collections and evaluations are listed in Table 2.

Analysis of the data sets was consistent with space groups *Pnma* and *P6̄2m* for NP- and HP-CePtSn, respectively. The isotypy with the orthorhombic TiNiSi [58] and the hexagonal ZrNiAl [59–61] type structures was evident from the powder data. The starting atomic positions were deduced from automatic interpretations of direct methods with SHELXS-97 [62], and both structures were refined using SHELXL-97 (full-matrix least-squares on *F*_o²) [63] with anisotropic displacement parameters for all sites. Refinement of the correct absolute structure of HP-CePtSn was ensured through refinement of the Flack parameter [64, 65]. The occupancy parameters of both crystals were refined in a separate series of least-squares cycles in order to check for the correct composition. They varied between 99.7(3)% for Pt and 100.3(4)% for Sn for NP-CePtSn and from 99.2(16)% for Sn and 101.5(15)% for Pt2 for HP-CePtSn. Thus, all sites were fully occupied within one standard deviation. In the last cycles, the ideal occupancies were assumed again. Final difference Fourier synthesis revealed no significant residual peaks (see Table 2). The positional parameters and interatomic distances are listed in Tables 3 and 4. Further details on the structure refinements may be obtained from Fachinformationszentrum Karlsruhe, D-76344 Eggenstein-Leopoldshafen (Germany), by quoting the Registry No.'s, CSD-415491 (NP-CePtSn) and CSD-415492 (HP-CePtSn).

Table 3. Atomic coordinates and anisotropic displacement parameters (pm²) for NP- and HP-CePtSn. *U*_{eq} is defined as one third of the trace of the orthogonalized *U*_{ij} tensor. The anisotropic displacement factor exponent takes the form $-2\pi^2[(ha^*)^2U_{11} + \dots + 2kha^*b^*U_{12}]$. *U*₂₃ = 0. The positional parameters of HP-CePtSn determined from the Rietveld refinement are given in italics.

Atom	Wyckoff position	<i>x</i>	<i>y</i>	<i>z</i>	<i>U</i> ₁₁	<i>U</i> ₂₂	<i>U</i> ₃₃	<i>U</i> ₁₂	<i>U</i> ₁₃	<i>U</i> _{eq}
CePtSn (normal-pressure phase)										
Ce	4 <i>c</i>	0.01216(7)	1/4	0.69585(7)	58(3)	80(3)	70(2)	0	4(2)	69(2)
Pt	4 <i>c</i>	0.29042(5)	1/4	0.40901(4)	82(2)	67(2)	67(2)	0	–1(1)	72(1)
Sn	4 <i>c</i>	0.17657(9)	1/4	0.08318(7)	75(3)	57(3)	59(3)	0	–1(2)	64(2)
CePtSn (high-pressure phase)										
Ce	3 <i>f</i>	0.5870(3) 0.5846(6)	0	0	76(6)	82(8)	78(10)	41(4)	0	78(4)
Pt1	1 <i>a</i>	0	0	0	90(6)	<i>U</i> ₁₁	43(11)	45(3)	0	74(4)
Pt2	2 <i>d</i>	2/3	1/3	1/2	91(4)	<i>U</i> ₁₁	80(9)	45(2)	0	87(4)
Sn	3 <i>g</i>	0.2513(3) 0.2526(7)	0	1/2	70(7)	66(10)	56(12)	33(5)	0	65(5)

Table 4. Interatomic distances (pm), calculated with the powder lattice parameters in NP- and HP-CePtSn. All distances of the first coordination sphere are listed.

Normal-pressure phase			High-pressure phase		
Ce:	1 Pt	310.0(1)	Ce:	4 Pt2	308.5(1)
	2 Pt	323.3(1)		1 Pt1	312.6(2)
	2 Sn	323.8(1)		2 Sn	328.1(2)
	1 Sn	334.0(1)		4 Sn	342.9(1)
	2 Pt	334.2(1)		4 Ce	395.3(1)
	1 Sn	336.0(1)		2 Ce	415.2(1)
	2 Sn	340.3(1)			
	1 Pt	357.5(1)			
	2 Ce	383.4(1)			
	2 Ce	390.6(1)			
Pt:	2 Sn	271.4(1)	Pt1:	6 Sn	281.6(1)
	1 Sn	274.8(1)		3 Ce	312.6(2)
	1 Sn	288.5(1)	Pt2:	3 Sn	288.4(1)
	1 Ce	310.0(1)		6 Ce	308.5(1)
	2 Ce	323.3(1)			
	2 Ce	334.2(1)			
	1 Ce	357.5(1)			
Sn:	2 Pt	271.4(1)	Sn:	2 Pt1	281.6(1)
	1 Pt	274.8(1)		2 Pt2	288.4(1)
	1 Pt	288.5(1)		2 Ce	328.1(2)
	2 Ce	323.8(1)		2 Sn	329.5(3)
	1 Ce	334.0(1)		4 Ce	342.9(1)
	1 Ce	336.0(1)			
	2 Ce	340.3(1)			

Electronic structure calculations

Self-consistent DFT band structure calculations were performed using the LMTO-method in its scalar-relativistic version (program TB-LMTO-ASA) [66]. Detailed descriptions are given elsewhere [67, 68]. Reciprocal space integrations were performed with the tetrahedron method [69] using 490 (NP-CePtSn) or 700 (HP-CePtSn) k -points within the irreducible wedges of the tetragonal Brillouin zones. The basis sets consisted of Ce: $6s/\{6p\}/5d/4f$, Pt: $6s/6p/5d/\{4f\}$ and Sn: $5s/5p/\{5d/4f\}$. Orbitals given in parentheses were downfolded [70]. In order to achieve space filling within the atomic sphere approximation, interstitial spheres are introduced to avoid too large overlap of the atom-centered spheres. The empty spheres positions and radii were calculated automatically. We did not allow overlaps of more than 15% for any two atom centered spheres. The COHP method was used for the bond analysis [71]. COHP gives the energy contributions of all electronic states for a selected bond. The values are negative for bonding and positive for antibonding interactions. With respect to the COOP diagrams, we plot $-\text{COHP}(E)$ to get positive values for bonding states.

Magnetic data of HP-CePtSn

The magnetic susceptibilities of a polycrystalline, powdered sample of HP-CePtSn were determined with a Quantum Design PPMS in the temperature range 2 to 300 K with

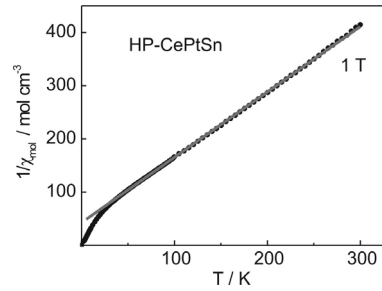


Fig. 3. Temperature dependence of the reciprocal magnetic susceptibility of HP-CePtSn measured in an external field of 1 T. The straight line corresponds to the Curie-Weiss fit.

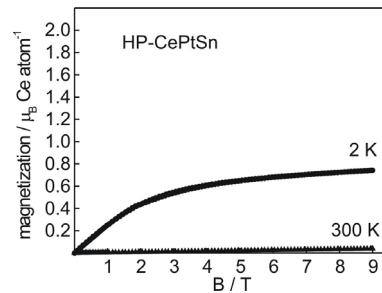


Fig. 4. Magnetization vs external flux density for HP-CePtSn at 2 and 300 K.

magnetic flux densities up to 9 T. 10.6 mg of the sample were enclosed in a small gelatin capsule and fixed at the sample holder rod. The sample was then cooled to 2 K in zero magnetic field and slowly heated to room temperature in the applied external field.

The temperature dependence of the reciprocal magnetic susceptibility is presented in Fig. 3. HP-CePtSn shows Curie-Weiss behavior above 40 K with an experimental magnetic moment of $2.55(1) \mu_B/\text{Ce atom}$, close to the free ion value [72] of $2.54 \mu_B$ for Ce^{3+} . The paramagnetic Curie temperature (Weiss constant) of $-35(1) \text{ K}$, determined by linear extrapolation of the $1/\chi$ vs T plot to $1/\chi = 0$, is indicative of antiferromagnetic interactions. The inverse susceptibility significantly deviates from Curie-Weiss behavior below 40 K, indicating crystal field splitting of the $J = 5/2$ ground state, but also the beginning of short range magnetic fluctuations. No magnetic ordering is evident down to 2 K.

The magnetization vs field behavior is presented in Fig. 4. At 300 K, the magnetization increases linearly with a very small value at 9 T, as expected for a paramagnetic material. At 2 K the magnetization shows a steeper increase, however, we do not observe saturation at the highest obtainable field of 9 T. The magnetization at 2 K and 9 T is only $0.74(1) \mu_B/\text{Ce atom}$, significantly reduced from the theoretical value for Ce^{3+} of $2.14 \mu_B$. This magnetic behavior is similar to CeRhSn_2 [73, 74]. The small value of the magnetic

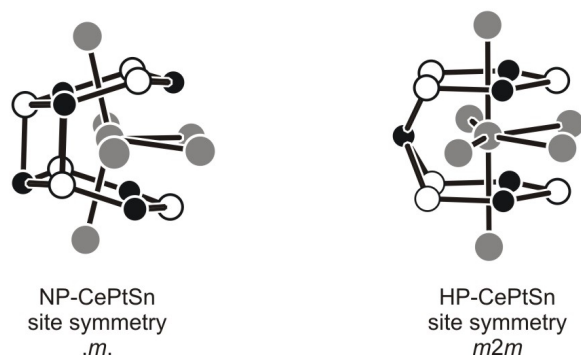


Fig. 6. Coordination polyhedra of the cerium atoms in NP-CePtSn and HP-CePtSn. The site symmetries are indicated.

with the present investigation. The U_{22} parameters of all three sites give absolutely no hint for a violation of the mirror plane perpendicular to the b axis.

Projections of the NP-CePtSn and HP-CePtSn structures along the short unit cell axis are presented in Fig. 5. From a geometrical point of view, both modifications are built up from platinum centered trigonal prisms that are formed by four cerium and two tin atoms for NP-CePtSn, while two Ce_6 and Sn_6 prisms are found for the Pt2 and Pt1 atoms of HP-CePtSn. The prisms show different patterns of condensation.

The shortest interatomic distances in both modifications occur between the platinum and tin atoms: 271–289 pm in NP-CePtSn and 282–288 pm in HP-CePtSn, close to or slightly longer than the sum of the covalent radii of 269 pm [79]. Together, the platinum and tin atoms build up three-dimensional networks of puckered hexagons as emphasized at the left-hand part of Fig. 5. The cerium atoms are located in slightly distorted hexagonal channels formed by these networks. They are bonded to the networks through relatively short Ce-Pt contacts of 310–323 pm (NP-CePtSn) and 308–313 pm (HP-CePtSn).

The most accented difference of the two modifications concerns the cerium coordination as emphasized in Fig. 6. Both cerium sites have six nearest cerium neighbors with an average Ce-Ce distance of 412 pm (range of 383–463 pm) in NP-CePtSn and 402 pm (range of 395–415 pm) in HP-CePtSn. The high-pressure phase clearly shows the smaller range and also the smaller average distance. Even more drastic is the situation for the Ce-Pt contacts with an average distance of 330 pm for the six platinum neighbors in NP-CePtSn and of 309 pm for the five platinum neighbors in HP-CePtSn. In contrast, the average Ce-

Sn distance of 338 pm in HP-CePtSn is slightly longer than in NP-CePtSn (333 pm).

A striking difference occurs for the platinum-tin coordination. In NP-CePtSn, each platinum atom has four nearest tin neighbors in a strongly distorted tetrahedral coordination with an average Pt-Sn distance of 277 pm, while there occur two crystallographically independent platinum sites in HP-CePtSn, both with significantly longer Pt1-Sn and Pt2-Sn distances of 282 pm (6 \times) and 288 pm (3 \times), respectively. The longer Pt1-Sn is comprehensible as suggested by the increased coordination number (pressure-distance paradoxon), but the longer Pt2-Sn distance with only three contacts is remarkable.

At this point it is worthwhile to compare the two modifications of CePtSn with α - and β -YbPdSn [80]. The latter stannide crystallizes with the hexagonal ZrNiAl type in the α -modification (low temperature) with essentially trivalent ytterbium and with the orthorhombic TiNiSi type in the β -modification (high temperature) with essentially divalent ytterbium. The course of the cell volumes of NP- and HP-CePtSn is consistent with these findings.

The change in structure type has no influence on the cerium valence. The experimental magnetic moment of HP-CePtSn in the paramagnetic regime clearly manifests trivalent cerium, similar to the NP modification [5]. Nevertheless, in contrast to the Néel temperature of 8 K for NP-CePtSn, we observe no magnetic ordering down to 2 K for HP-CePtSn. Since we do not observe a change of the cerium valence, also the other orthorhombic $REPtSn$ ($RE = La, Pr, Nd, Sm$) stannides are supposed to transform to a hexagonal high-pressure modification. Investigations of these and other TiNiSi type $CeTX$ intermetallics are in progress.

In order to compare the differences in electronic structure and chemical bonding of HP- and NP-CePtSn, we have performed spin-polarized DFT band structure calculations and analyzed the bonds by the COHP method. The self consistent field (SCF) calculations of HP-CePtSn converge to a metallic ground state as expected. The resulting theoretical magnetic moment is compatible with one unpaired spin localized at the Ce atom, which is in agreement with the experimental magnetic moment of $2.55(1) \mu_B$ and confirms again the trivalent state of cerium. Fig. 7 shows the COHP diagrams of the Pt-Sn, Ce-Pt and Ce-Sn interactions, which surely amount to the main part of the bonding energy of these structures. For clarity, we do not distinguish between crystallographically different

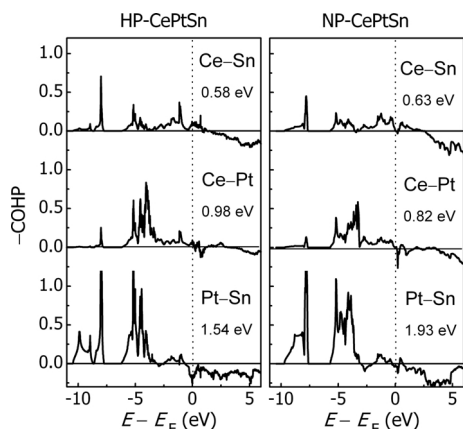


Fig. 7. Crystal Orbital Hamilton Population (COHP) diagrams of the major bonds in HP- and NP-CePtSn. The mean integrated (ICOHP) energies per bond are given in eV; the energy zero is taken at the Fermi level.

bonds. Each of the COHP curves and integration values represent a weighted average of multiple (similar) bonds and thereby allows to compare their strengths directly. In both cases, we find the Pt–Sn bonds to be the by far strongest, which agrees with the idea of a covalent $[\text{PtSn}]^{3-}$ substructure. The distorted tetrahedral tin coordination in NP-CePtSn splits into one sixfold and one threefold coordinated Pt. But the latter one occurs twice in the unit cell, and thus we count the same number of four Pt–Sn bonds per formula unit. Using the different bond frequencies, the COHP diagram reveals that the Pt–Sn bonds get considerably (–25%) weaker in the high pressure phase, whereas the Ce–Pt bonds get only slightly weaker (–6%) and finally the Ce–Sn bonds are stronger (+12%). If we multiply the ICOHP energies/bond by their frequency of occurrence per formula unit, we obtain total covalent ICOHP bonding energies of 16.4 eV for NP-CePtSn and 15.5 eV for HP-CePtSn. This is attributed to the weaker Pt–Sn bonds and to the loss of one Ce–Pt contact in HP-CePtSn. Such a decrease of covalent bond-

ing energy is typical for high-pressure phases and corresponds to a further metallization of all bonds due to the volume reduction. But altogether we find that the total binding energies of NP- and HP-CePtSn are remarkably similar despite the drastic changes in the coordination geometries. Also the total energy of the normal pressure structure is almost identical to that of the high-pressure variant and differs only by 0.78 eV/cell. Volume dependent calculations predict no phase transition from NP- to HP-CePtSn, *i.e.* NP-CePtSn remains more stable at pressures up to 20 GPa, but strictly only at $T = 0$ K. However, from this we expect that no structural transition under pressure will occur at room temperature. We approximate the volume reduction for NP-CePtSn from the calculated bulk module to be about –9% at 10 GPa. Thus the unit cell volume under ambient conditions of 68.66 \AA^3 will be compressed to 62.5 \AA^3 at 10 GPa. This is smaller than the volume of GdPtSn with 64.84 \AA^3 , which already adopts the hexagonal structure of HP-CePtSn. From this we conclude, that although NP- and HP-CePtSn form different structures, both have nearly the same stabilities. We conclude that the activation energy to transform one to the other is very high and can only be overcome by applying high temperature and high pressure conditions simultaneously. This is also supported by the remarkable stability of HP-CePtSn upon heating up to 850 °C, before it transforms back to the more stable NP-CePtSn.

Acknowledgements

We thank Prof. W. Schnick for using the high-pressure facilities, Dipl.-Chem S. Correll for the *in-situ* X-ray diffraction, H.-J. Göcke for the work at the scanning electron microscope, and Dipl.-Ing. U. Ch. Rodewald for help with the intensity data collections. This work was financially supported by the Deutsche Forschungsgemeinschaft (Po573/10-1 and HU966/4-1) and the European Science Foundation through the COST D30/003/03 network *Development of Materials Chemistry using High-Pressures*.

- [1] T. Fujita, T. Suzuki, S. Nishigori, T. Takabatake, H. Fujii, J. Sakurai, *J. Magn. Magn. Mater.* **108**, 35 (1992).
- [2] A. Szytuła, J. Leciejewicz, *Handbook of Crystal Structures and Magnetic Properties of Rare Earth Intermetallics*. CRC Press, Boca Raton, Florida (1994).
- [3] R. Kraft, R. Pöttgen, D. Kaczorowski, *Chem. Mater.* **15**, 2998 (2003).
- [4] E. Gaudin, B. Chevalier, B. Heying, U. Ch. Rodewald, R. Pöttgen, *Chem. Mater.* **17**, 2693 (2005).
- [5] J. Sakurai, Y. Yamaguchi, S. Nishigori, T. Suzuki, T. Fujita, *J. Magn. Magn. Mater.* **90&91**, 422 (1990).
- [6] I. Higashi, K. Kobayashi, T. Takabatake, M. Kasaya, *J. Alloys Compd.* **193**, 300 (1993).
- [7] M. Kolenda, J. Leciejewicz, N. Stuesser, A. Szytuła, A. Zygmunt, *J. Magn. Magn. Mater.* **145**, 85 (1995).
- [8] D. Rafaja, V. Rejdák, B. Janoušová, P. Svoboda, V. Sechovský, *J. Alloys Compd.* **334**, 50 (2002).
- [9] B. Janoušová, P. Svoboda, V. Sechovský, K. Prokeš, T. Komatsubara, H. Nakotte, S. Chang, B. Ouladdiaf, I. Čisářová, *Appl. Phys. A: Mater. Sci. & Processing* **74**, S731 (2002).
- [10] Y. Yamaguchi, J. Sakurai, F. Teshima, H. Kawanaka,

- T. Takabatake, H. Fujii, *J. Phys.: Condens. Matter* **2**, 5715 (1990).
- [11] M. Kyogaku, Y. Kitaoka, H. Nakamura, K. Asayama, F. Teshima, T. Takabatake, H. Fujii, Y. Yamaguchi, J. Sakurai, *J. Magn. Magn. Mater.* **90&91**, 487 (1990).
- [12] M. Kasaya, T. Tani, H. Suzuki, K. Ohoyama, M. Kohgi, *J. Phys. Soc. Jpn.* **60**, 2542 (1991).
- [13] Ch. D. Routsis, J. K. Yakinthos, *J. Magn. Magn. Mater.* **110**, 317 (1992).
- [14] J. Sakurai, R. Kawamura, T. Taniguchi, S. Nishigori, S. Ikeda, H. Goshima, T. Suzuki, T. Fujita, *J. Magn. Magn. Mater.* **104–107**, 1415 (1992).
- [15] H. Kadowaki, T. Ekino, H. Iwasaki, T. Takabatake, H. Fujii, J. Sakurai, *J. Phys. Soc. Jpn.* **62**, 4426 (1993).
- [16] S. Nishigori, H. Goshima, T. Suzuki, T. Fujita, G. Nakamoto, T. Takabatake, H. Fujii, J. Sakurai, *Physica B* **186–188**, 406 (1993).
- [17] M. Kohgi, K. Ohoyama, T. Osakabe, M. Kasaya, T. Takabatake, H. Fujii, *Physica B* **186–188**, 409 (1993).
- [18] T. Takabatake, H. Iwasaki, G. Nakamoto, H. Fujii, H. Nakotte, F. de Boer, V. Sechovský, *Physica B* **183**, 108 (1993).
- [19] S. Nohara, H. Namatame, A. Fujimori, T. Takabatake, *Phys. Rev. B* **47**, 1754 (1993).
- [20] G. M. Kalvius, A. Kratzer, K. H. Münch, F. E. Wagner, S. Zwirner, H. Kobayashi, T. Takabatake, G. Nakamoto, H. Fujii, S. R. Kreitzmann, R. Kiefl, *Physica B* **186–188**, 412 (1993).
- [21] S. Nohara, H. Namatame, A. Fujimori, T. Takabatake, *Physica B* **186–188**, 403 (1993).
- [22] G. M. Kalvius, K. Kratzer, K.-H. Münch, T. Takabatake, G. Nakamoto, H. Fujii, R. Wäppling, H. H. Klauß, R. Kiefl, S. Kreitzmann, D. R. Noakes, *Hyp. Int.* **85**, 411 (1994).
- [23] M. Diviš, H. Nakotte, F. de Boer, P. de Châtel, V. Sechovský, *J. Phys.: Condens. Matter* **6**, 6895 (1994).
- [24] D. T. Adroja, B. D. Rainford, *Physica B* **194–196**, 363 (1994).
- [25] H. Kobayashi, F. E. Wagner, G. M. Kalvius, T. Takabatake, *Hyp. Int.* **93**, 1515 (1994).
- [26] Y. Bando, T. Takabatake, H. Tanaka, H. Iwasaki, H. Fujii, S. K. Malik, *Physica B* **194–196**, 1179 (1994).
- [27] G. M. Kalvius, A. Kratzer, D. R. Noakes, K. H. Münch, R. Wäppling, H. Tanaka, T. Takabatake, R. F. Kiefl, *Europhys. Lett.* **29**, 501 (1995).
- [28] T. J. Hammond, G. A. Gehring, M. B. Suvasini, W. M. Temmermann, *Phys. Rev. B* **51**, 2994 (1995).
- [29] M. Bazela, M. Kolenda, J. Leciejewicz, N. Stuesser, A. Szytuła, A. Zygmunt, *J. Magn. Magn. Mater.* **140–144**, 881 (1995).
- [30] T. Suzuki, H. Fujisaki, T. Fujita, G. Nakamoto, T. Takabatake, H. Fujii, A. Tamaki, *J. Magn. Magn. Mater.* **140–144**, 1215 (1995).
- [31] G. M. Kalvius, D. R. Noakes, A. Kratzer, K. H. Münch, R. Wäppling, H. Tanaka, T. Takabatake, R. F. Kiefl, *Physica B* **206&207**, 205 (1995).
- [32] T. Takabatake, T. Nakamoto, T. Yoshino, H. Fujii, M. Sera, Tohoku Daigaku Kinzoku Zairyo Kenkyusho Kyojiba Chodendo Zairyo Kenkyu Senta Nenji Hokoku 257 (1996).
- [33] D. T. Adroja, B. D. Rainford, A. J. Neville, A. G. M. Jansen, *Physica B* **223&224**, 275 (1996).
- [34] A. Kratzer, *Appl. Magn. Res.* **13**, 137 (1997).
- [35] H. Kadowaki, *J. Phys. Soc. Jpn.* **67**, 3261 (1998).
- [36] H. Kadowaki, *J. Phys. Chem. Solids* **60**, 1199 (1999).
- [37] G. M. Kalvius, A. Kratzer, G. Grosse, D. R. Noakes, R. Wäppling, H. von Löhneysen, T. Takabatake, Y. Echizen, *Physica B* **289–290**, 256 (2000).
- [38] H. Nakotte, S. Chang, M. S. Torikachvili, H. N. Bordallo, A. H. Lacerda, T. Takabatake, *Physica B* **281&282**, 103 (2000).
- [39] D. R. Noakes, G. M. Kalvius, *Physica B* **289–290**, 248 (2000).
- [40] T. Khmelevska, P. Svoboda, B. Janoušová, V. Sechovský, S. Chang, H. Nakotte, M. S. Torikachvili, *J. Appl. Phys.* **89**, 7189 (2001).
- [41] T. Khmelevska, S. Chang, H. Nakotte, P. Svoboda, M. S. Torikachvili, V. Sechovský, *J. Alloys Compd.* **323–324**, 380 (2001).
- [42] K. Shimada, K. Kobayashi, T. Narimura, P. Baltzer, H. Namatame, M. Taniguchi, T. Suemitsu, T. Sasakawa, T. Takabatake, *Phys. Rev. B* **66**, 155202 (2002).
- [43] J. Kitagawa, T. Sasakawa, T. Suemitsu, Y. Echizen, T. Takabatake, *Phys. Rev. B* **66**, 224304 (2002).
- [44] B. Janoušová, V. Rejčák, P. Svoboda, M. Diviš, D. Rafaja, V. Sechovský, *Czech. J. Phys.* **52**, 259 (2002).
- [45] K. Shimada, K. Kobayashi, T. Narimura, P. Baltzer, H. Namatame, M. Taniguchi, T. Suemitsu, T. Sasakawa, T. Takabatake, *Physica B* **329–333**, 576 (2003).
- [46] B. Janoušová, V. Sechovský, K. Prokeš, T. Komatsubara, *Physica B* **328**, 145 (2003).
- [47] B. Janoušová, J. Kulda, M. Diviš, V. Sechovský, T. Komatsubara, *Physica B* **335**, 26 (2003).
- [48] T. Takabatake, T. Sasakawa, J. Kitagawa, T. Suemitsu, Y. Echizen, K. Umedo, M. Sera, Y. Bando, *Physica B* **328**, 53 (2003).
- [49] B. Janoušová, J. Kulda, M. Diviš, V. Sechovský, T. Komatsubara, *Phys. Rev. B* **69**, 220412 (2004).
- [50] R. Pöttgen, Th. Gulden, A. Simon, *GIT-Laborfachzeitschrift* **43**, 133 (1999).
- [51] H. Huppertz, *Z. Kristallogr.* **219**, 330 (2004).
- [52] D. Walker, M. A. Carpenter, C. M. Hitch, *Am. Mineral.* **75**, 1020 (1990).
- [53] D. Walker, *Am. Mineral.* **76**, 1092 (1991).

- [54] D. C. Rubie, *Phase Trans.* **68**, 431 (1999).
- [55] K. Yvon, W. Jeitschko, E. Parthé, *J. Appl. Crystallogr.* **10**, 73 (1977).
- [56] T. Roisnel, J. Rodríguez-Carvajal, Fullprof.2k V. 2.0 (2001) Laboratoire Léon Brillouin (CEA-CNRS), 91191 Gif-sur-Yvette Cedex (France).
- [57] J.-F. Béjar, P. Lelann, *J. Appl. Crystallogr.* **24**, 1 (1991).
- [58] C. B. Shoemaker, D. P. Shoemaker, *Acta Crystallogr.* **18**, 900 (1965).
- [59] P. I. Kropyakevich, V. Ya. Markiv, E. V. Melnyk, *Dopov. Akad. Nauk. Ukr. RSR, Ser. A* **750** (1967).
- [60] A. E. Dwight, M. H. Mueller, R. A. Conner, Jr., J. W. Downey, H. Knott, *Trans. Met. Soc. AIME* **242**, 2075 (1968).
- [61] M. F. Zumdick, R.-D. Hoffmann, R. Pöttgen, *Z. Naturforsch.* **54b**, 45 (1999).
- [62] G. M. Sheldrick, SHELXS-97, Program for the Determination of Crystal Structures, University of Göttingen, Germany (1997).
- [63] G. M. Sheldrick, SHELXL-97, Program for Crystal Structure Refinement, University of Göttingen, Germany (1997).
- [64] H. D. Flack, G. Bernadinelli, *Acta Crystallogr. A* **55**, 908 (1999).
- [65] H. D. Flack, G. Bernadinelli, *J. Appl. Crystallogr.* **33**, 1143 (2000).
- [66] O. K. Andersen, O. Jepsen, Tight-Binding LMTO Vers. 4.7, Max-Planck-Institut für Festkörperforschung, Stuttgart (1994).
- [67] O. Jepsen, M. Snob, O. K. Andersen, *Linearized Band Structure Methods and its Applications*, Springer Lecture Notes, Springer-Verlag, Berlin (1987).
- [68] H. L. Skriver, *The LMTO Method*, Springer-Verlag, Berlin (1984).
- [69] O. K. Andersen, O. Jepsen, *Solid State Commun.* **9**, 1763 (1971).
- [70] W. R. L. Lambrecht, O. K. Andersen, *Phys. Rev. B* **34**, 2439 (1986).
- [71] R. Dronskowski, P. Blöchl, *J. Phys. Chem.* **97**, 8617 (1993).
- [72] H. Lueken, *Magnetochemie*, Teubner, Stuttgart (1999).
- [73] D. Niepmann, R. Pöttgen, B. Künnen, G. Kotzyba, C. Rosenhahn, B. D. Mosel, *Chem. Mater.* **11**, 1597 (1999).
- [74] Z. Hossain, L. C. Gupta, C. Geibel, *J. Phys.: Condens. Matter* **14**, 9687 (2002).
- [75] R. Pöttgen, *Z. Naturforsch.* **51b**, 806 (1996).
- [76] J. Sakurai, K. Kegai, T. Kuwai, Y. Isikawa, K. Nishimura, K. Mori, *J. Magn. Magn. Mater.* **140–144**, 875 (1995).
- [77] F. Canepa, S. Cirafici, *J. Alloys Compd.* **232**, 71 (1996).
- [78] A. E. Dwight, W. C. Harper, C. W. Kimball, *J. Less-Common Met.* **30**, 1 (1973).
- [79] J. Emsley, *The Elements*, Oxford University Press, Oxford (1999).
- [80] D. Kußmann, R. Pöttgen, B. Künnen, G. Kotzyba, R. Müllmann, B. D. Mosel, *Z. Kristallogr.* **213**, 356 (1998).